International Conference on Mathematics and Computational Methods Applied to Nuclear Science and Engineering (M&C 2011)
Rio de Janeiro, RJ, Brazil, May 8-12, 2011, on CD-ROM, Latin American Section (LAS) / American Nuclear Society (ANS)
ISBN 978-85-63688-00-2

CONDITIONAL PROBABILITY DISTRIBUTION ASSOCIATED TO THE E-M IMAGE RECONSTRUCTION ALGORITHM FOR NEUTRON STIMULATED EMISSION TOMOGRAPHY

Viana R. S.*, Yoriyaz H. and Santos A.
Instituto de Pesquisas Energéticas e Nucleares, IPEN/CNEN-SP
Av. Lineu Prestes, 2242, Cidade Universitária, P.O. Box 11049, 05508-000 São Paulo, Brazil
rodrigossviana@gmail.com; hyoriyaz@ipen.br; asantos@ipen.br

ABSTRACT

The Expectation-Maximization (E-M) algorithm is an iterative computational method for maximum likelihood (M-L) estimates, useful in a variety of incomplete-data problems. Due to its stochastic nature, one of the most relevant applications of E-M algorithm is the reconstruction of emission tomography images. In this paper, the statistical formulation of the E-M algorithm was applied to the *in vivo* spectrographic imaging of stable isotopes called Neutron Stimulated Emission Computed Tomography (NSECT). In the process of E-M algorithm iteration, the conditional probability distribution plays a very important role to achieve high quality image. This present work proposes an alternative methodology for the generation of the conditional probability distribution associated to the E-M reconstruction algorithm, using the Monte Carlo code MCNP5 and with the application of the reciprocity theorem.

Key Words: E-M algorithm, emission computed tomography, MCNP5, Monte Carlo code, NSECT.

1. INTRODUCTION

The Expectation-Maximization (E-M) algorithm is a generally used approach to the iterative computation of maximum likelihood (M-L) estimates in a variety of incomplete-data problems. The major idea of the E-M algorithm is to associate an incomplete-data problem with a complete-data problem in which M-L estimation is easier to solve. In this way, the methodology of the E-M algorithm consists in rewrite the problem based on the incomplete-data set in terms of the complete-data problem, establishing a relationship between the likelihoods of these two problems and evaluates the maximum likelihood estimate (MLE) of the complete-data problem [1].

One of the most relevant applications of E-M algorithm is the reconstruction of tomography images. The results are considered more reliable with respect to the object reconstructed than that obtained with other analytical methods of reconstruction due to the stochastic nature associated with the formulation of the E-M algorithm, represented by maximum likelihood. In this paper, the statistical formulation of the E-M algorithm was applied to the emission computed tomography considering an object containing an isotropic radiation source.

* Corresponding author

In recent years, a new technique for *in vivo* spectrographic imaging of stable isotopes was presented as Neutron Stimulated Emission Computed Tomography (NSECT) [2,3]. In this technique, using multiple projections, a fast neutron beam interacts with the stable isotopes of the irradiated tissue, through inelastic scatterings, making them jump into an excited state. When they return to their ground state, they emit photons which energies are intrinsic to the emitting nuclei. The emitted gamma energy spectra can be used for two purposes: (a) reconstruction of the target tissue image and; (b) determination of the tissue elemental composition. Considering a clinical application, the spatial distribution of the several stable isotopes that compose the body can be used in the study of the tissues metabolism [4,5].

In this present work the details of the E-M reconstruction algorithm for NSECT is described. An emphasis was given to an analysis of the intrinsic aspects on the acquisition of conditional probability distribution associated to the E-M reconstruction related to geometric shapes, as well as to the differentiation among compositions according to the emission of photons generated in the reaction of inelastic scattering.

2. METHODS

2.1. The E-M algorithm

Let $\boldsymbol{Y}$ be the random vector corresponding to the incomplete-data $\boldsymbol{y}$ (observed data), having a probability density function (p.d.f.) given by $g(\boldsymbol{y};\boldsymbol{\psi})$, where $\boldsymbol{\psi} = (\psi_1, \ldots, \psi_d)^T$ is the transpose vector of unknown parameters in space $\boldsymbol{\Omega}$. The function $g_c(\boldsymbol{x};\boldsymbol{\psi})$ denotes the p.d.f. of the random vector $\boldsymbol{X}$ corresponding to the complete-data vector $\boldsymbol{x}$. If $\boldsymbol{x}$ were fully observable, the logarithm of the complete-data likelihood function, $L_c(\boldsymbol{\psi})$, that could be formed by $\boldsymbol{\psi}$, is given by:

$$\log L_c(\boldsymbol{\psi}) = \log \prod_{\boldsymbol{\psi}} \prod_{\boldsymbol{x}} g_c(\boldsymbol{x},\boldsymbol{\psi}) . \tag{1}$$

Formally, there are two samples spaces χ and γ, respectively, referring to the complete-data $\boldsymbol{x}$ and incomplete-data $\boldsymbol{y}$ and these two samples spaces have a univocal relationship, i.e., for $\boldsymbol{x} \in \chi$ there is a $\boldsymbol{y}=\boldsymbol{y}(\boldsymbol{x}) \in \gamma$. In this way, instead of observing the complete-data vector $\boldsymbol{x}$ in χ, it's possible to observe the incomplete-data vector $\boldsymbol{y} = \boldsymbol{y}(\boldsymbol{x})$ in γ, according to:

$$g(\boldsymbol{y};\boldsymbol{\psi}) = \int_{\chi(\boldsymbol{y})} g_c(\boldsymbol{x},\boldsymbol{\psi}) d\boldsymbol{x}, \tag{2}$$

where, $\chi(\boldsymbol{y})$ is the subset of χ determined by the equation $\boldsymbol{y} = \boldsymbol{y}(\boldsymbol{x})$.

The E-M algorithm approaches the problem of solving the incomplete-data likelihood indirectly by proceeding iteratively in terms of the complete-data log likelihood function, $\log L_c(\boldsymbol{\psi})$. As it is unobservable, it is replaced by its conditional expectation given $\boldsymbol{y}$, using the current $\boldsymbol{\psi}$.

The E-M iteration algorithm is composed by two steps: the expectation step (E-step) and the maximization step (M-step). Let $\boldsymbol{\psi}^{(0)}$ be the initial value for $\boldsymbol{\psi}$. In the first iteration, the E-step requires the calculation of the complete-data log likelihood function expectation $\log L_c(\boldsymbol{\psi})$ with respect to the observed data $\boldsymbol{y}$:

$$Q(\boldsymbol{\psi};\boldsymbol{\psi}^{(0)}) = E_{\boldsymbol{\psi}^{(0)}}\{\log L_c(\boldsymbol{\psi}) \mid \boldsymbol{y}\}. \tag{3}$$

Then, the M-step performs the maximization of $Q(\boldsymbol{\psi};\boldsymbol{\psi}^{(0)})$ with respect to $\boldsymbol{\psi}$ over the space $\boldsymbol{\Omega}$. That is, it does choose $\boldsymbol{\psi}^{(1)}$ such that:

$$Q(\boldsymbol{\psi}^{(1)};\boldsymbol{\psi}^{(0)}) \geq Q(\boldsymbol{\psi};\boldsymbol{\psi}^{(0)}), \tag{4}$$

for all $\boldsymbol{\psi} \in \boldsymbol{\Omega}$.

On the $(k+1)^{\text{th}}$ iteration the E- and M-steps are defined as follows:

E-step. Calculate $Q(\boldsymbol{\psi};\boldsymbol{\psi}^{(k)})$:

$$Q(\boldsymbol{\psi};\boldsymbol{\psi}^{(k)}) = E_{\boldsymbol{\psi}^{(k)}}\{\log L_c(\boldsymbol{\psi}) \mid \boldsymbol{y}\}. \tag{5}$$

M-step. Choose $\boldsymbol{\psi}^{(k+1)}$ to be any value of $\boldsymbol{\psi} \in \boldsymbol{\Omega}$ that maximizes $Q(\boldsymbol{\psi};\boldsymbol{\psi}^{(k)})$:

$$Q(\boldsymbol{\psi}^{(k+1)};\boldsymbol{\psi}^{(k)}) \geq Q(\boldsymbol{\psi};\boldsymbol{\psi}^{(k)}). \tag{6}$$

The E- and M-steps are alternated repeatedly until the difference $\boldsymbol{\psi}^{(k+1)} - \boldsymbol{\psi}^{(k)}$ becomes smaller than a predetermined value or until another convergence criterion be satisfied [6].

2.2. E-M reconstruction algorithm for emission computed tomography

The E-M algorithm has been employed in M-L estimation of parameters in computerized image reconstruction process such as SPECT (Single-photon Emission Computed Tomography) or PET (Positron Emission Tomography). On emission computed tomography the goal is to estimate the local intensities of photon emission in the object of interest. The used statistical modeling assumes that emissions occur according to a Poisson process in the region under study with an unknown intensity function, usually referred to as the emission density. The algorithm is defined following the notation described in [1].

The space over which the reconstruction is required is divided into a number n rectangular pixels, and it is assumed that the unknown emission density in the i^{th} pixel (i=1, …,n) is λ_i. Let y_j denote the number of counts recorded in the j^{th} projection (j=1, …, d), where d denotes the number of projections. At this point it is necessary to emphasize that the counts recorded on d

projections are obtained with a proper positioning of the detection system and under the same uncertainty σ_j. Wrong detector's setup can influence the quality of reconstruction, because photon countings that are not produced by the irradiated object may cause additional noise in the true counts, which is related to the photons produced by the interaction of neutrons scattered in the detectors, photons scattered between the detectors and secondary photons produced by the interaction of high energy photons scattered in the detectors through pair production. The assumption that the obtained counts y_j made by detectors under the same uncertainty σ_j is necessary for the stochastic uncertainty propagation does not interfere with image reconstruction.

The reconstruction aims to infer the transpose vector of emission densities $\boldsymbol{\lambda} = (\lambda_1, \ldots, \lambda_n)^T$ using the vector of the observable counts $\boldsymbol{y} = (y_1, \ldots, y_d)^T$. Given the vector $\boldsymbol{\lambda}$ of stable isotope densities, the counts $y_1, \ldots, y_d$ are conditionally independent according to a Poisson distribution, namely:

$$Y_j \sim P(\mu_j), \tag{7}$$

where, the mean μ_j of Y_j is given by:

$$\mu_j = \sum_{i=1}^{n} \lambda_i p_{ij} \qquad (j = 1, \ldots, d), \tag{8}$$

and, p_{ij} is the conditional probability distribution that a photon is counted at the j^{th} projection given that it was emitted from within the i^{th} pixel.

The conditional probability distribution plays a very important role in the algorithm iteration process and its correct determination implies the consideration of the physical characteristics of the tomography system and of the object to be reconstructed itself, since it depends basically on the geometry and positioning of the detectors and on the location and concentration of stable isotopes.

The complete-data vector in this example is $\boldsymbol{x} = (\boldsymbol{y}^T, \boldsymbol{z}^T)^T$, where the vector $\boldsymbol{z}$ consists of the unobservable data, which in this formulation are the missing counts. The vector $\boldsymbol{z}$ is composed by z_{ij} defined to be the number of photons emitted within pixel i and recorded at the j^{th} projection ($i = 1, \ldots, n$; $j = 1, \ldots, d$). It is assumed that, given $\boldsymbol{\lambda}$, the Z_{ij} are conditionally independent, with each Z_{ij} having a Poisson distribution specified as:

$$Z_{ij} \sim P(\lambda_i p_{ij}) \qquad (i = 1, \ldots, n; j = 1, \ldots, d). \tag{9}$$

The complete-data log likelihood is given by:

$$\log L_c(\boldsymbol{\lambda}) = \sum_{i=1}^{n} \sum_{j=1}^{d} \left\{ -\lambda_i p_{ij} + z_{ij} \log\left(\lambda_i p_{ij}\right) - \log z_{ij}! \right\}. \tag{10}$$

The Poisson distribution belongs to the linear exponential family, so that, the equation (10) is linear in the unobservable data Z_{ij}. In this way, the E-step on the $(k + 1)^{\text{th}}$ iteration requires the calculation of the conditional expectation of Z_{ij} given the observed data $\boldsymbol{y}$, using the current $\boldsymbol{\lambda}^{(k)}$

for $\boldsymbol{\lambda}$. The conditional distribution of Z_{ij} given $\boldsymbol{y}$ and $\boldsymbol{\lambda}^{(k)}$ is a binomial distribution with sample size parameter y_j and probability parameter given by:

$$P(Z_{ij}|\mathbf{y}, \boldsymbol{\lambda}^{(k)}) = \frac{\lambda_i p_{ij}}{\sum_{h=1}^{n} \lambda_h p_{hj}} \qquad (i = 1, \ldots, n; j = 1, \ldots, d). \tag{11}$$

The expected value for a parameter that has a binomial distribution is given by the product of its sample size and its occurrence probability, so, using the equation 11 follows that:

$$E_{\boldsymbol{\lambda}^{(k)}}(Z_{ij} \mid \mathbf{y}) = \frac{y_j \lambda_i^{(k)} p_{ij}}{\sum_{h=1}^{n} \lambda_h^{(k)} p_{hj}} = z_{ij}^{(k)}. \tag{12}$$

With z_{ij} replaced by $z_{ij}^{(k)}$ in equation 10, the application of the M-step on the $(k + 1)^{\text{th}}$ iteration gives:

$$\lambda_i^{(k+1)} = q_i^{-1} \sum_{j=1}^{d} E_{\boldsymbol{\lambda}^{(k)}}(Z_{ij} \mid \mathbf{y})$$

$$\lambda_i^{(k+1)} = \lambda_i^{(k)} q_i^{-1} \sum_{j=1}^{d} \left\{ \frac{y_j p_{ij}}{\sum_{h=1}^{n} \lambda_h^{(k)} p_{hj}} \right\} \quad (i = 1, \ldots, n), \text{ where } q_i = \sum_{j=1}^{d} p_{ij}\,. \tag{13}$$

Note that the vector of emission densities $\boldsymbol{\lambda}$ is estimated from the vector of the observable counts $\boldsymbol{y}$ considering that they are conditionally independent according to a Poisson distribution and that the conditional distribution of the vector of unobservable data $\boldsymbol{z}$ assumes a binomial distribution. Based on properties of these two distributions, they are equivalent in a particular case where the Poisson distribution parameter is equal to the expected value for the binomial probability parameter. This equality can be verified using equations 8 and 12. Since $y_j = \sum_{h=1}^{n} \lambda_h p_{hj}$ follows that:

$$\lambda_i p_{ij} = \frac{y_j \lambda_i p_{ij}}{\sum_{h=1}^{n} \lambda_h p_{hj}}\,. \tag{15}$$

This fact implies that estimates of the new complete-data vector and the emission densities vector $\boldsymbol{\lambda}$ are simultaneously performed in accordance with the conditional probability distribution p_{ij}. Assuming that all the physical features of the tomography system are related with p_{ij}, the next section will be dedicated to its formulation and to the description of the simulated tomography system using the Monte Carlo code MCNP5.

2.3. Monte Carlo method

The Monte Carlo method (MCM) can be described as a statistical method, which uses a sequence of random numbers to perform a simulation. In terms of radiation transport, the stochastic process can be seen as a family of particles moving randomly in each individual collision as they travel through matter. The average behavior of these particles is described in terms of macroscopic quantities such as flux or particle density. The expected value of these quantities corresponds to the deterministic solution of the Boltzman equation. Specific quantities such as deposited energy or dose are derived from these quantities.

In practical applications of the MCM, the physical process is simulated directly, without solving the mathematical equations representing the system behavior. The only requirement needed is that the physical process can be described by a probability density function, which models the physical process of the observed phenomenon. Thus, the essence of MCM applied to radiation transport is to estimate quantities, observing the behavior of a large number of individual events [7].

The MCNP code is a well-known and widely used Monte Carlo code for neutron, photon, and electron transport simulations [8]. The first MCNP version was released in the mid-1970s for neutron and photon transport, and was enhanced over the years to include generalized sources and tallies, electron physics and coupled electron-photon calculations, macrobody geometry, statistical convergence tests and other features. The present work utilized the last MCNP released version which is the version 5. The MCNP5 particle transport simulation requires an input file (inp), which allows the user to specify all the information about geometry modeling, source specifications, material compositions, and the specific quantities to be estimated (tallies).

2.3.1. MCNP5 setup simulations

A geometric phantom was proposed to be able to evaluate the performance of the reconstruction algorithm to solve edges and corners, as well as the differentiation between different compositions. Simultaneously to the image reconstruction, using the spectrum of emitted photons, it is possible to infer the isotopic composition of the irradiated medium by the correspondence between the prominent peaks of energy and the energy differences between the excited states of stable isotopes. The proposed geometric phantom is shown in Figure 1.

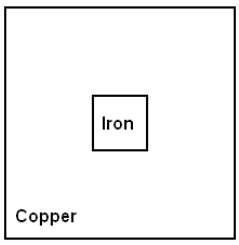

Figure 1. Geometric phantom composed by iron and copper cubes with edges 1 and 6 cm respectively.

The tomographic system was simulated considering the structure of a first generation tomography. An important detail of the NSECT, in contrast to conventional computed tomography, is that the detectors are positioned in such a way to avoid neutron detection, but only scattered photons. The configuration adopted in the simulations of the detectors is shown in Figure 2.

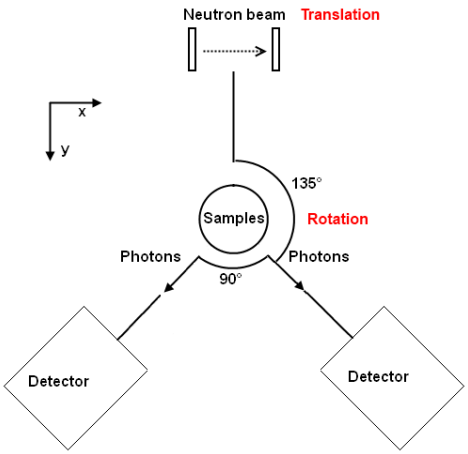

Figure 2. NSECT configuration setup for Monte Carlo simulation.

Two hyper-pure germanium (HPGe) detectors were modeled as cylinders of 5.32 g/cm^3 density with 12 cm diameter and 15 cm height. The detectors were separated 90° from each other and both forms 135° with the neutron beam axis, as shown in Figure 2. The neutron source was modeled in MCNP5 as a monoenergetic energy beam of 7.5 MeV and with a rectangular section of 1.0 x 0.1 cm^2. This neutron source can typically be obtained through the fusion reactions d + T and d + D [9].

Natural abundance occurrence has been considered for the iron and copper compositions. The phantom is is kept fixed while detectors and the neutron source are rotated in intervals of 5° performing 72 angular positions. In each evaluated angular position the neutron source is translated 15 steps. All tomographic system is immersed in air. For each source motion, 2x10^8 histories have been simulated and photons whose emission was stimulated by inelastic scattering of fast neutron beam were recorded on the surface of the detectors.

2.3.2. Conditional probability distribution p_{ij} and stimulated photon emission

NSECT uses a thin beam of fast neutrons to stimulate stable nuclei in a sample, which emit characteristic gamma radiation. The photon energy is unique and is used to identify the emitting nuclei. The results are tomographic images and spectroscopy of elements distribution in the body acquired through a non-invasive *in vivo* scan [10].

When a neutron collides with an atomic nucleus, several nuclear reactions may occur. Among them, one of the most probable interactions is the inelastic scattering. When the neutron scatters

inelastically, part of the neutron energy is transferred to the nucleus leaving it in an excited state. After several picoseconds, the excited state decays to a lower state, until the ground state, usually emitting photons. The probability of a photon to be emitted from the i^{th} voxel and to be detected in the j^{th} projection is associated with the geometry and composition of the irradiated object, the energy of the neutron beam and the geometry and configuration of the detectors. These factors affect production, attenuation and scattering of produced photons in the reaction of inelastic scattering.

The Monte Carlo solution of each voxel-projection pair configuration problem will give the voxel importance factor for that configuration which can be associated to the conditional probability. However, the number of configuration problems to be solved is dictated by the number of voxels which usually is very large, requiring excessively high computational time. To circumvent this problem it was assumed that the reciprocity theorem is valid [11]. In other words, it was assumed that the probability associated to a photon to be emitted from the i^{th} voxel and to be detected in the j^{th} projection is equivalent to a photon to be emitted from the j^{th} projection and to be detected in the i^{th} voxel. Using the reciprocity theorem, the neutron source has a well-defined line of response with the voxels that lie in the neutron beam path into a virtual mesh. In other words, in each evaluated projection, the neutron beam is collimated so that each projection there is a given probability distribution associated with the set of pixels that are in the neutron beam path. Therefore, the E-M reconstruction algorithm uses the probability distribution p_{ij} to associate the obtained counts from the j^{th} projection with the pixels set under the same orientation of the neutron beam. This procedure reduced significantly the Monte Carlo simulations since the number of projections is much smaller than the number of voxels.

2.3.3. Counts and photon flux

The tomographic system modeling requires the calculation of the number of photons produced by inelastic scattering reaction that reaches the detectors in each projection, as well as of the neutron flux inside the tomographic field of vision (FOV). For this purpose we used, respectively, the F1 and F4 tallies available on MCNP5. The F1 tally counts the number of particles crossing a specified surface, which in this case are detector's surfaces. The number of particles at time t in a volume element $d\mathbf{r}$, with directions within solid angle $d\boldsymbol{\Omega}$, and energies within dE is $n(\mathbf{r}, \boldsymbol{\Omega}, E, t)d\mathbf{r}d\boldsymbol{\Omega}dE$. Let the volume element $d\mathbf{r}$ contain the surface element dA (with surface normal n) and along Ω for a distance vdt. The differential volume element is $d\mathbf{r} = vdt\left|\boldsymbol{\Omega}\cdot n\right| dA$. All the particles within this volume element with directions within $d\boldsymbol{\Omega}$ and energies within dE will cross surface dA in time dt. So, the number of particles crossing surface A in energy bin i, time bin j, and angle bin k is:

$$F1 = \int_{E_i} dE \int_{t_j} dt \int_{\boldsymbol{\Omega}_k} d\boldsymbol{\Omega} \int dA \left|\boldsymbol{\Omega}\cdot n\right| vn(\mathbf{r},\boldsymbol{\Omega},E,t). \tag{16}$$

The scalar flux is defined by $\phi(\mathbf{r},E,t) = \int d\boldsymbol{\Omega}\psi(\mathbf{r},\boldsymbol{\Omega},E,t)$, so that, $\phi(\mathbf{r},E,t)d\mathbf{r}dE$ is the total scalar flux in volume element $d\mathbf{r}$ about $\mathbf{r}$ and energy element dE about E. The F4 tally estimates the flux in a defined volume V, in an energy bin i, and in a time bin j, such that:

$$F4 = \frac{1}{V}\int_{E_i} dE \int_{t_j} dt \int dV \phi(\mathbf{r}, E, t)\,. \tag{17}$$

Associated with the F4 tally, the neutron flux was estimated using the FMESH option available in MCNP5. This option allows the creation of a superimposed virtual mesh over any defined volume, considering the geometry, composition and location of internal structures.

3. RESULTS AND DISCUSSION

The E-M reconstruction algorithm was developed in MATLAB® [12] environment using three limits on the number of iterations: 5, 10, 15 and 20. It is known from the literature that while the E-M algorithm moves toward convergence, after a certain number of iterations the resulting solution starts to degrade, becoming noisier than the previous one [13]. At this point, the algorithm should be stopped to avoid the image deterioration. Figures 3a, b c and d show the reconstructed images, respectively, with 5, 10, 15 and 20 iterations. As can be seen, the four reconstructions have characteristics from air-copper interface and the only factor that differentiates them is the number of iterations. Due to the previously discussed characteristic of the E-M algorithm, the number of iterations affects the image quality and it should be chosen according to the characteristics of the final image to be generated and also taking in account contrast and brightness levels. In the present simulations, there is a significant difference between the inelastic scattering cross sections of the metals that make up the phantom and the air, besides, the regions corresponding to metals are extensive and well defined.

These features require a high-contrast image and the tomographic reconstruction that best meets that condition was obtained with 20 iterations (Figure 3d). Figure 3a shows a blurred effect between air-copper and iron-copper interfaces and Figures 3b and 3c have appropriate brightness and contrast but not show so well defined edges and corners as in Figure 3d. If we were interested in resolving internal structures within the metallic samples, Figure 3d would not be the best choice but Figure 3b or 3a, because these figures do not show as much noise as in Figure 3d, which is intrinsic to the stochastic reconstruction method. Figure 3 shows a magnification of some regions of interest as discussed in the four reconstructions. In these magnifications is possible notice the influence of the number of iterations in the image reconstruction quality.

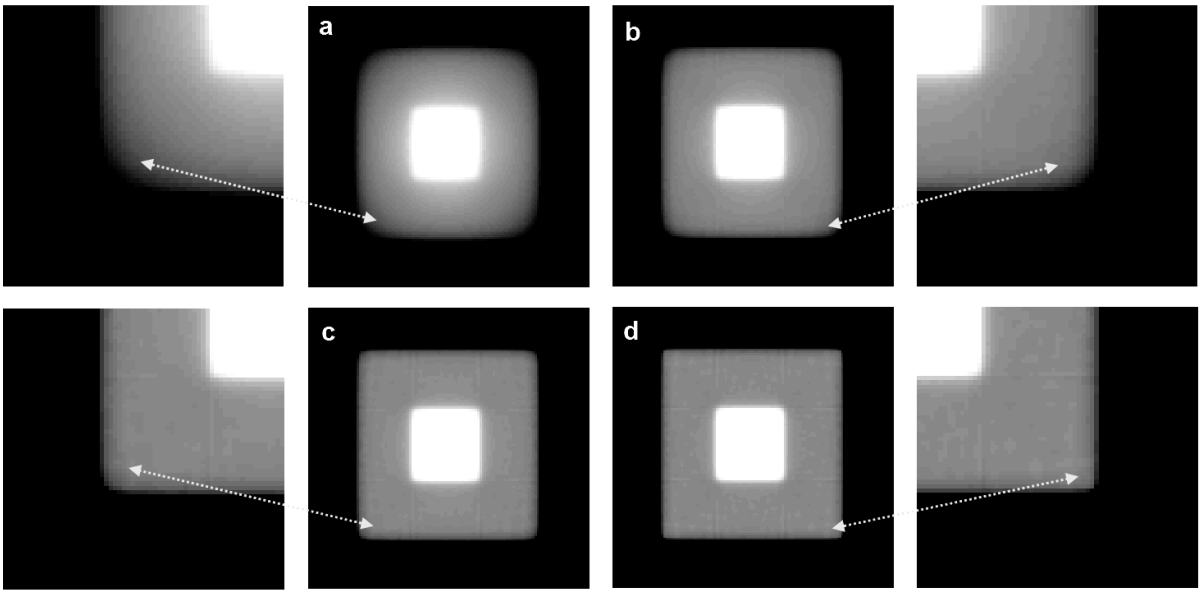

Figure 3. Reconstructed images obtained in a 128 x 128 pixel grid: (a) 5, (b) 10, (c) 15 and (d) 20 iterations.

As shown in the formulation of the E-M reconstruction algorithm, the counts obtained in each projection are distributed according to the conditional probability distribution p_{ij}. As already described, the conditional probability distribution relates the abundance of the emission of photons with the spatial distribution of the isotopes of interest. While the algorithm is running, the estimated emission density λ_i is iteratively updated according to the estimate of the new complete-data vector, which in addition is characterized by the observed and unobserved data (undetected photons). Thus, according to equation 14, each iteration provides an estimative of a new complete-data vector which updates the observed counts. Figure 4 shows the observed counts updating according to the neutron source translations perpendicular to phantom side.

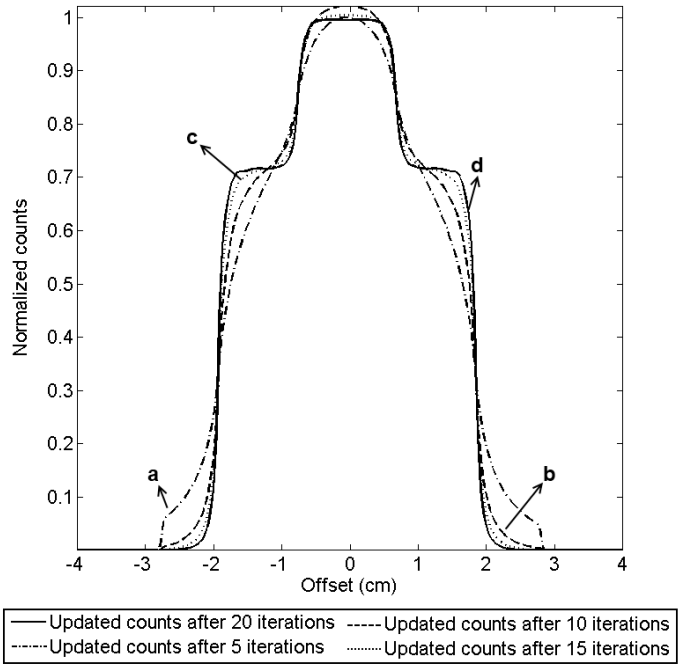

Figure 4. Updated counts by the E-M algorithm. Labels *a, b, c* and *d* are corresponding to the reconstructed images shown in Figure 3.

One of the main features of NSECT that make its study and development very interesting is related to the ability to obtain simultaneously the spatial distribution of stable isotopes and estimates of the isotopic composition of the irradiated medium. This is done matching the correspondence between the spectrum of emitted photons and energy differences between the excited states of the isotopes under investigation. Breast cancer detection and evaluation of iron overload in the liver are some of the applications successfully performed with the analysis of changes in the isotopic composition using the spectrum of the scattered photons stimulated by fast neutrons. In these applications, the equivalent dose was estimated to be 0.498 mSv for breast and 0.239 mSv for liver [14-16].

To illustrate this application, in addition to the tomographic reconstruction of the image which is the spatial distribution of stable isotopes, the spectrum of photons emitted by the simulated phantom and recorded on the surface of the detectors was obtained with an energy bin width of ± 2 keV. The characteristic photopeaks produced by different isotopes present in the phantom were compared to the data using a lookup table from the National Nuclear Database [17]. The spectrum obtained is shown in Figure 5 and the correspondence between the identified peaks and the evaluated isotopes are described in Table I.

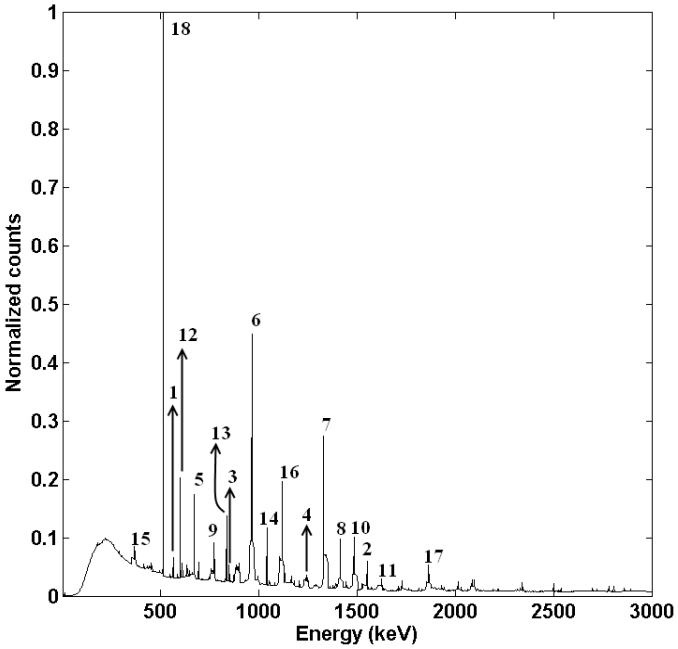

Figure 5. Scattered photons spectrum recorded on the surface of the detectors. Labels are provided for those peaks that matched elements found in the modeled geometric phantom.

Table I. Isotopes and their corresponding peaks in the simulated spectrum.

Isotope	Energy (keV)	Peak	Percentual relative error (%)
Fe^{56}	846	3	0.65
	1238	4	0.80
Fe^{54}	1550	2	0.61
Fe^{57}	569	1	0.60
Cu^{63}	669	5	0.36
	962	6	0.22
	1327	7	0.29
	1412	8	0.48
	1861	17	0.66
Cu^{65}	770	9	0.50
	1481	10	0.49
	1623	11	0.88
Ge^{74}	595	12	0.34
Ge^{70}	1039	14	0.45
	1117	16	0.35
	834	13	0.41
	364	15	0.53
Pair Production	511	18	0.16

As can be seen, the spectrum has energies whose maximum counts refer to the characteristics energies of emitted photons by the simulated phantom and detectors. Yet, due to the high energy of the emitted photons, we could detect the energy resulting from the pair production occurring in the detectors and at the phantom itself.

4. CONCLUSIONS

The simulated technique for *in vivo* spectrographic imaging of stable isotopes NSECT is well-founded and, given its potential, has a wide application in medical and biological research. In this imaging modality the spatial distribution of stable isotopes can be retrieved by image reconstruction and due to its stochastic nature the E-M algorithm has been used for this purpose. In the E-M formulation, the conditional probability distribution assumes an important role in the iteration process since it relates the abundance of the emission of photons with the spatial distribution of isotopes of interest.

The present work proposed a methodology for the acquisition of the conditional probability distribution based on the reciprocity theorem. It requires the calculation of the number of photons whose emission was stimulated by inelastic scattering of fast neutron beam recorded on the surface of the detectors and the neutron flux inside the tomographic FOV. To achieve this purpose the F1 and F4 flux tallies available on MCNP5 were used.

The F1 tally estimates the number of particles crossing the detector's surfaces. The F4 estimates the neutron flux inside the object and it was used in association with the FMESH card, which has the property to create a superimposed virtual mesh over defined volumes. So each voxel created by FMESH card is associated with F4 tally and in this way, the neutron flux inside the tomographic FOV is estimated according to neutron source orientation, assuming that the neutron source has a well-defined line of response with the voxels that lie in the neutron beam path into a virtual mesh. The methodology demonstrated to be effective and presented good results with regard to the quality and reliability of the reconstructed images, given the physical characteristics of metals irradiated by fast neutron beam represented by the layout and cross section of inelastic scattering of metallic samples.

ACKNOWLEDGMENTS

This work was supported by Fundação de Amparo à Pesquisa do Estado de São Paulo – FAPESP, grant no 2010/04206-4.

REFERENCES

1. G. McLachlan, T. Krishnan, The EM Algorithm and Extensions, John Wiley & Sons, New York, USA (1997).
2. C. Floyd Jr, J. Bender, A. Sharma, A. Kapadia, J. Xia, B. Harrawood, G. Tourassi, J. Lo, A. Crowell, C. Howell, "Introduction to neutron stimulated emission computed tomography," *Phys. Med. Biol.*, **51**, pp.3375-3390 (2006).
3. C. Floyd Jr, A. Sharma, J. Bender, A. Kapadia, J. Xia, B. Harrawood, G. Tourassi, J. Lo, M. Kiser, A. Crowell, R. Pedroni, R. Macri, S. Tajima, C. Howell, "Neutron stimulated emission computed tomography: Background corrections," *Nuclear Instruments and Methods in Physics Research B*, **254**, pp.329-336 (2007).
4. C. Floyd Jr, A. Kapadia, J. Bender, A. Sharma, J. Xia, B. Harrawood, G. Tourassi, J. Lo, A. Crowell, M. Kiser, C. Howell, "Neutron-stimulated emission computed tomography of a multi-element phantom," *Phys. Med. Biol.*, **53**, pp.2313-2326 (2008).
5. A. Sharma, B. Harrawood, J. Bender, G. Tourassi, A. Kapadia, "Neutron stimulated emission computed tomography: a Monte Carlo simulation approach," *Phys. Med. Biol*, **52**, pp.6117-6131 (2007).
6. A. Dempster, N Laird, D. Rubin, "Maximum Likelihood from Incomplete Data via the EM Algorithm," *Journal of the Royal Statistical Society Series B*, **39**, pp.1-38 (1977).
7. H. Yoriyaz, "Monte Carlo Method: principles and applications in Medical Physics," *Revista Brasileira de Física Médica*, **3**, pp.141-149.
8. F. Browm, R. Barrett, T. Booth, J. Bull, L. Cox, R. Forster, T. Goorley, R. Mosteller, S. Post, R. Prael, E. Selcow, A. Sood, J. Sweezy, "MCNP Version 5," *Applied Physics Division - Los Alamos National Laboratory*, **LA-UR-02-3935**, (2002).
9. Internation Commission on Radiation Units and Measurements, "*Clinical Neutron Dosimetry Part I: Determination of Absorbed Dose in a Patient Treated by External Beams of Fast Neutron*", **ICRU REPORT 45**, (1989).
10. C. Floyd Jr, C. Howell, B. Harrawood, A. Crowell, A. Kapadia, R. Macri, J. Xia, R. Pedroni, J. Bowsher, M. Kiser, G. Tourassi, W. Tornow, R. Walter, "Neutron Stimulated Emission Computed Tomography of Stable Isotopes," *Proceedings of SPIE*, Bellingham, **53**, Vol. 5368, pp.248-254 (2004).
11. R. Loevinger, *Radiation dosimetry*, Academic Press, New York, USA (1969).
12. MATLAB version R2009b. Natick, Massachusetts: The MathWorks Inc., 2010.
13. J. Kay, "The EM algorithm in medical imaging," *Statistical Methods in Medical Research*, **6**, pp.55-75 (1997).
14. A. Kapadia, G. Tourassi, A. Sharma, A. Crowell, M. Kiser, C. Howell, "Experimental detection of iron overload in liver through neutron stimulated emission spectroscopy," *Phys. Med. Biol.*, **53**, pp.2633-2649 (2008).
15. J. Bender, A. Kapadia, A. Sharma, G. Tourassi, B. Harrawood, C. Floyd Jr, "Breast cancer detection using neutron stimulated emission computed tomography: Prominent elements and dose requirements," *Med. Phys*, **34**, pp.3866-3871 (2007).
16. A. Kapadia, A. Sharma, G. Tourassi, J. Bender, C. Howell, C. Floyd Jr, C. Howell, A. Crowell, M. Kiser, B. Harrawood, R. Pedroni, "Neutron Stimulated Emission Computed Tomography for Diagnosis of Breast Cancer," *IEEE Transactions on Nuclear Science*, **55**, pp.501-509 (2008).
17. "National Nuclear Data Center BNL, NuDat 2.5," http://www.nndc.bnl.gov/nudat2/ (2010).